Simultaneous seasonal dry/wet signals in Eastern and Central Asia since the Last Glacial Maximum

Simin Peng[1], Yu Li[1], Zhansen Zhang[1], Mingjun Gao[1], Xiaowen Chen[1], Junjie Duan[1], Yaxin Xue[1]

5   [1]Key Laboratory of Western China's Environmental Systems (Ministry of Education), College of Earth and Environmental Sciences, Center for Hydrologic Cycle and Water Resources in Arid Region, Lanzhou University, China

Correspondence to: Yu Li (liyu@lzu.edu.cn)

Abstract. The East Asian monsoon region with the summer precipitation regime and the Mediterranean climate region with the winter precipitation regime show opposite dry/wet changes since the Last Glacial Maximum (LGM). Therefore, different

10 precipitation regimes bring about the opposing changes in dry/wet states between Eastern and Central Asia (EA and CA). Based on a comprehensive study of modern observational datasets, ensemble simulations of eight climate models from the Paleoclimate Model Intercomparison Project phase 3 (PMIP3), and a compilation of 42 proxy records from EA and CA, here we assess the relationship of seasonal precipitation signals involving rain and heat periods and the difference and linkage in dry/wet states from EA and CA. At short-term timescales, empirical orthogonal function (EOF) analysis results of mean annual

15 precipitation show the spatial diversity of overall precipitation pattern in EA and CA. However, EOF results of summer and winter precipitation indicate the similarity between EA and the east of CA, suggesting that seasonal signals of precipitation affected by the Asian monsoon, westerlies, ENSO, NAO, and PDO are the primary factor causing the linkage in dry/wet states.

At long-term timescales, reconstructed dry/wet states from proxy records since the LGM reveal parallel evolutionary feature in EA and the east of

CA as well. A visual inspection from PMIP3 multi-model simulations in summer and winter shows that the insolation in

20 different seasons control the intensity of westerlies and summer monsoon and further influence the summer and winter precipitation in EA and CA since the LGM. Overall, we suggest, in addition to the traditional difference caused by different precipitation regimes, that dry/wet states in EA and CA universally have inter-regional connections affected by seasonal signals of precipitation at multiple time scales.

1 Introduction

25 As typical midlatitude climatic regions, Eastern and Central Asia (EA and CA) are commonly featured with vigorous circulations and are dominated by two atmospheric systems, namely midlatitude westerlies and Asian monsoon (Li, 1990; Zhang and Lin, 1992; Chen et al., 2008; Nagashima et al., 2011). These two regions are generally characterized by opposite climate and

environment changes, embodied in water resources, vegetation cover and ecosystems, which gives rise to their different response to climate change (Sorg et al., 2012; Zhang and Feng, 2018). CA, where precipitation is scarce throughout

30 the year, is the largest arid region in the mid-latitudes dominated by westerlies (Chen et al., 2009; Huang et al., 2015a). On the contrary, affected by the Asian summer monsoon that carries water vapor from the Pacific and Indian Ocean, the monsoon-dominated EA receives more precipitation (Wang et al., 2017). These contrasting climate regimes have attracted much research interest.

Over the past few years, there have been many comparative studies for dry/wet changes in EA and CA on a range of time scales, e.g., orbital, millennial, interdecadal timescales and annual timescales. Early works suggested that the climate change mode of

35 'cold-wet' or 'warm-dry' occurred in northwestern China during the last glacial/interglacial cycle, which is different from the 'cold-dry' or 'warm-wet' modes of the monsoon climate (Li, 1990; Han and Qu, 1992; Han et al., 1993). In monsoonal EA, a strengthened summer monsoon and humid climate usually occur in the early and mid Holocene, and a weakened summer monsoon and drier climate prevailed during the late Holocene (Dykoski et al., 2005; Chen et al., 2015). Based on the integration of paleoclimate records, modern meteorological observation data and paleoclimate simulations, Chen et al. (2008, 2009, 2019)

40 revealed that the 'westerlies-dominated climatic regime' in arid CA presents dry early Holocene, wetter mid-Holocene, and moderately wet late Holocene, which is out-of-phase or anti-phased with dry/wet states in the monsoon-dominated regions. However, paleoclimate records in some regions of CA indicate an asynchronous climate history, in contradiction with dry/wet changes caused by the westerlies (An et al., 2006; Zhao et al., 2015; Wang et al., 2018). More recent studies proposed that the persistent weakening of the East Asian summer monsoon since 1958 causes an increasing contribution of the

45 monsoonal water vapor transport, thereby enhancing summer precipitation in arid CA on the annual timescale (Chen et al., 2021a; Chen et al., 2021b). Therefore, further research is needed to explain dry/wet changes in different regions and explore the difference and linkage in climate change modes from EA and CA at multiple time scales.

The seasonal signals of precipitation, derived from the simultaneity of rain and heat periods, is an important climate phenomenon on seasonal to orbital time scales. It involves enhanced precipitation at a seasonal scale during northern hemisphere summer and during warm period on long-

50 term timescales. Reduced precipitation occurs during northern hemisphere winter and during long-term cold periods. This study aims to focus on the transitional zone in the arid and semi-arid region of eastern CA where the westerlies and the monsoon interact with the summer precipitation regime being similar as in the monsoon-dominated EA. Utilizing modern observations,

paleoclimate proxies, and model simulations, we conducted a comprehensive analysis of changes in dry/wet states in EA and CA since annual to millennial time scales based on seasonal signals of precipitation.

2 Materials and methods

55

2.1 Study area

In this study, we divide the boundaries of CA and EA mainly according to the modern Asian summer monsoon limit defined by Chen et al. (2008, 2019). CA is the largest arid and semi-arid area in the mid-latitude hinterland of the Eurasian continent, extending from the Caspian Sea in the west to the western Hexi Corridor in the east, comprising the central Asian countries, NW China, and southern Mongolian Plateau (Fig. 1). Considering that the strength and trajectory of monsoon circulation is a major control of moisture in EA, the regional scope of EA for this study is defined as the Chinese monsoon region in the east and south of the modern Asian summer monsoon limit in Chin (Fig. 1). We calculated the precipitation difference between the summer (April to September) and winter (October to March) half year between

1971 and 2020, and defined the region greater than 0 mm as an area of simultaneous rain and heat periods. Therefore, we

65 define the simultaneous region of rain and heat periods in CA as the east of CA (Fig. 1). The seasonality perspective implies that different precipitation regimes could affect the difference and linkage in climate change modes from EA and CA at the multi-time scale. Taking seasonal signals as the dividing criteria, the core region of CA is characterized by a wet cold-season climate, whereas EA and the east of CA are characterized by a wet warm-season climate (Fig. 1).
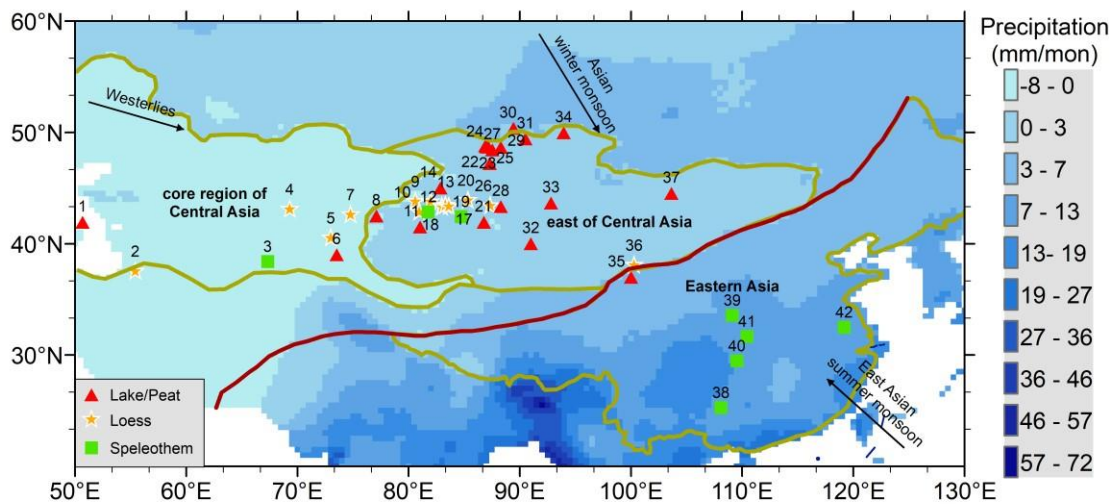
70   **Figure 1.** Overview map showing the paleoclimate record sites selected in this study from EA and CA, the difference between summer and winter precipitation over 1965-2014 (shade), and the dominant circulation systems, including the westerlies, Asian winter monsoon and East Asian summer monsoon. The modern Asian summer monsoon limit (red solid line) is summarized by Chen et al. (2008, 2019). The brown solid line represents the range of CA, the core region of CA, the east of CA, and EA as defined in this study.

2.2 Modern observation and analytical methods

The monthly high-resolution (0.5°×0.5°) land precipitation data (referred to as CRU TS4.06) are selected from a Climatic Research Unit (CRU) updated gridded climate dataset from the University of East Anglia (van der Schrier et al., 2013; Harris et al., 2014; Barichivich et al., 2021). The CRU monthly climate archives are obtained from the auspices of the World Meteorological Organization (WMO) and the US National Oceanographic and Atmospheric Administration (NOAA, via its National Climatic Data Center, NCDC). The Global Reanalysis 1 datasets include monthly mean geopotential height, zonal wind, and meridional wind and is collected from the National Centers for Environmental Prediction/National Center for Atmospheric Research (NCEP/NCAR) (Kalnay et al., 1996). The reanalysis datasets have a horizontal resolution of 2.5° in latitude and longitude and a vertical resolution of 17 pressure levels from 1000 to 10 hPa. The high-resolution monthly averaged data for the vertical integral water vapor from the European Centre for Medium-Range Weather Forecasts (ECMWF; reanalysis v5 (ERA5)), intending to be used as a meteorological forcing dataset for land surface and hydrological models, is used in this study. This dataset covers the period from 1979 to the present with a spatial resolution of 0.25° in latitude and longitude and a single level integrated from the surface to the top of the atmosphere (Hersbach et al., 2020).

We used the National Center for Environmental Information (NCEI) Pacific Decadal Oscillation (PDO) index based on NOAA's extended reconstruction of SSTs (ERSST Version 5) to analyze long-lived El Niño-like pattern of Pacific climate variability (Zhang et al. 1997; Mantua and Hare, 2002). The data can be obtained at https://www.ncei.noaa.gov/pub/data/cmb/ersst/v5/index/ersst.v5.pdo.dat. The Niño 3.4 index is the most commonly used index to define El Niño and La Niña events. We selected the Niño 3.4 of area-averaged SST from 5°S-5°N and 170-120°W using the HadISST1 dataset (Rayner et al., 2003). The data can be obtained at https://psl.noaa.gov/gcos_wgsp/Timeseries/Nino34/. Positive values of the North Atlantic Oscillation (NAO) index are typically associated with stronger midlatitude westerlies and increased water vapor content from the North Atlantic. We used the Hurrell NAO index (station-based) to investigate the impact of NAO on midlatitude westerlies (Hurrell, 1995; Hurrell and Deser, 2009). The data can be obtained at https://climatedataguide.ucar.edu/sites/default/files/202210/nao_station_monthly.txt. Empirical orthogonal function (EOF) is a powerful method for dimensionality reduction and pattern extraction. EOF can decompose multidimensional climate data from different locations into spatial (EOF modes) and temporal functions (principal components). Therefore, to investigate the spatiotemporal variations of precipitation at the interannual timescale over EA and CA, the EOF analysis was applied to the CRU TS4.06 gridded precipitation data and ERA5 vertical integral water vapor. We focused on the first two leading modes that objectively account for the majority of dry/wet changes in EA and CA (Lorenz, 1956).

2.3 Calculation of Monsoon and westerly wind indices

105 The East Asian summer monsoon index (EASMI) is defined as the 850 hPa average summer meridional wind speed from June

to August over (27°N~37°N, 110°E~120°E) encompassing the East Asian summer monsoon domain (Liu et al., 2014). The

equation is as follows:

$\text{EASMI} = \vec{V}_{850}$ (27°~37°N, 110°~120°E)   (1) The westerly wind index (WWI) is

defined as the zonal difference of the 500 hPa averaged geopotential height over

110 (35°N~50°N, 70°E~110°E) (Li et al., 2008). The equation is as follows:

$$\text{WWI} = \overline{H_{35°}} - \overline{H_{50°}} = \frac{1}{17}\left[\sum_{\gamma=1}^{17} H(\gamma, 35°N) - \sum_{\gamma=1}^{17} H(\gamma, 50°N)\right] \qquad (2)$$

where H is the 500 hPa average height geopotential, γ is the number of longitudes taken along the latitude circle with a

spacing of 2.5°.

The East Asian winter monsoon index (EAWMI) is defined as the difference between the 300 hPa averaged zonal wind speed

115 from December to February over (27.5°~37.5°N, 110°~170°E) and (50°~60°N, 80°~140°E) (Jhun and Lee, 2004). The

equation is as follows:

$\text{EAWMI} = \vec{U}_{300}$ (27.5°~37.5°N, 110°~170°E) $- \vec{U}_{300}$ (50°~60°N, 80°~140°E)   (3) The

calculation of EASMI, WWI, and EAWMI all rely on the NCEP Reanalysis 1 dataset.

2.4 Regional paleoclimatic proxy data

120 Here we compiled various paleoclimate records to reconstruct long-term climate variability and primarily

paid close attention to paleo-precipitation and moisture changes since the LGM. We set three criteria to collect all the

published proxy records from EA and CA in our study. Firstly, the records should be located primarily in the intersection

encompassing the simultaneous region of rain and heat periods in EA and CA, which is in favour of investigating the

difference and linkage in climate change modes from EA and CA. Accordingly, some typical records climatologically

influenced by midlatitude

125 westerlies and East Asian summer monsoon in core regions of CA and EA were selected for comparative analysis. Secondly,

the proxies should be clearly indicative of changes in effective moisture or precipitation which have been confirmed by the

original investigators. Third, the record length should cover most of the period since the LGM without documented

depositional hiatuses. Fourth, the fluctuation and variation of proxy records should be predominantly forced by climate

change, rather than human activities (Manoj et al., 2020; Chen et al., 2021c, 2022). Following the above criteria, a total of 42

proxy records from

130 lakes, peats, loess, and stalagmites since the LGM were compiled for EA and CA (Fig. 1), enabling us to comprehensively

review the LGM moisture evolution of the region. To avoid the effect of chronological anomalies, this study usually selects

paleoclimate records with at least five chronological. In light of seasonal signals of precipitation, 35 records are from the

summer precipitation region, and seven records are from the winter precipitation region. Differences in geographic location,

hydrological setting, depositional proxies used, and sensitivities prevented linear comparisons between individual records

(Chen et al., 2008), so ordered humidity classes are specified to investigate dry/wet states in this study. We divided the LGM

into four time points: LGM (22-19 cal ka BP), early Holocene (EH, 11.7-8.2 cal ka BP), mid Holocene (MH, 8.2-4.2 cal ka

BP), late Holocene (LH, 4.2-0 cal ka BP). Dry/wet conditions were coded on the basis of effective moisture in the original

literature: wet, dry, moderately wet, and moderately dry respectively, which indicates the period of wetter, dryer and moderate

status at that particular site during the LGM (Fig. 4). Detailed information about these selected proxy records is presented in

Table S1.

2.5 Paleoclimatic simulations

135 The Paleoclimate Modelling Intercomparison Project (PMIP) was launched to coordinate and encourage the systematic study

of General Circulation Models (GCMs) and to understand the mechanisms of climate change and the role of climate feedback

(Joussaume et al., 1999) (Table 1). Eight coupled GCMs covering the LGM or MH from the PMIP3 database were selected to

analyze the mechanisms of climate change in this study (Table 2), including bcc-csm1-1, CNRM-CM5, CCSM4, CSIRO-

Mk3-

6-0, GISS-E2-R, MIROC-ESM, FGOALS-s2, and MRI-CGCM3. The output data of the PMIP3 in the LGM and MH are

140 available at htQTPs://esgf-node.llnl.gov/search/esgf-llnl/. By interpolating various climate variables on the common

1°×1° grid and then sorting the values of model simulations from minimum to maximum, we extracted the median value of

all PMIP3 models used in this paper to evaluate the PMIP3 model simulations and acquire the scientific model simulation

value.

Table 1. Boundary conditions and forcing for PMIP3-CMIP5 models at the LGM and MH.

Period	Eccentricity	Obliquity (°)	Longitude of perihelion (°)	CO_2 (ppm)	CH_4 (ppb)	N_2O (ppb)	Ice sheet	Vegetation
LGM	0.018994	22.949	114.425	185	350	200	Peltier (2004), 21 ka	Present day
MH	0.018682	24.105	0.87	280	650	270	Peltier (2004), 0 ka	Present day

Table 2. Basic information about climate models from PMIP3-CMIP5 used in this study.

Model	Institute	Resolutions	Variables[*]	References
bcc-csm1-1	Beijing Climate Center, China Meteorological Administration, China	64×128 (17)	ua, va, zg, hus, psl, pr, tas	Randall et al. (2007)
CNRM-CM5	Centre National de Recherches Météorologiques, France	128×256 (17)	ua, va, zg, hus, psl, pr, tas	Voldoire et al. (2013)
CCSM4	National Center for Atmospheric Research, USA	288×192 (17)	ua, va, zg, hus, psl, pr, tas	Gent et al. (2011)
CSIRO-Mk3-6-0	Australian Commonwealth Scientific and Industrial Research Organization Marine and Atmospheric Research in collaboration with the Queensland Climate Change Centre of Excellence, Australia	96×192 (18)	ua, va, zg, hus, psl, pr, tas	Rotstayn et al. (2010)
GISS-E2-R	NASA Goddard Institute for Space Studies, USA	144×90 (17)	ua, va, zg, hus, psl, pr, tas	Schmidt et al. (2014)
MIROC-ESM	Japan Agency for Marine-Earth Science and Technology, Japan	128×64 (35)	ua, va, zg, hus, psl, pr, tas	Watanabe et al. (2011)
FGOALS-s2	LASG-CEES. China	108×128 (17)	ua, va, zg, hus, psl, pr, tas	Briegleb et a1. (2004)
MRI-CGCM3	Meteorological Research Institute, Japan	320×160 (23)	ua, va, zg, hus, psl, pr, tas	Yukimoto et al. (2012)

[*]: ua means eastward_wind; va means northward wind; zg geopotential Height; hus near-surface relative humidity; psl means sea surface pressure; pr means precipitation;

tas means near-surface temperature.

3 Results

3.1 Seasonal signals at short-term timescales

To obtain the spatial distribution characteristics of the precipitation anomalies in EA and CA under the context of seasonal

signals, we conducted an EOF analysis on the precipitation standardized anomaly field over 1971-2020. Figure S1a-d shows

the spatial distribution and time series of EOF decomposition of mean annual precipitation. The center of negative values is in the core region of CA mainly belonging to the winter precipitation regime, while the positive values are in the south and north of EA located in summer precipitation regions (Fig. S1a). This opposite distribution indicates that the difference in the mean annual precipitation exists between EA and CA. Additionally, the first mode exhibits interdecadal and interannual changes

155 according to the PC1 (Fig. S1b). The second mode indicates that the center of positive values is in the north of EA, and the center of negative values is in the north of CA, also displaying the spatial diversity of mean annual precipitation in EA and CA (Fig. S1c).

In order to further explore the contribution of seasonal signals of precipitation to dry/wet conditions in EA and CA, we conducted

EOF analysis on spring, summer, autumn, and winter precipitation data. The variance contribution rate of the first mode in

160 precipitation of four seasons is shown in Fig. 2. The first mode of spring and autumn precipitation does not show obvious distribution characteristics, and the contribution rate is relatively uniform, indicating that spring and autumn precipitation have no special precipitation contribution to EA and CA (Fig. 2a and c). In relation to summer precipitation, centers of positive values are mainly distributed in the north of EA and the east of CA, while the negative values are mainly distributed in the core regions of CA and in central EA (Fig. 2b). But similar EOF results between CA and south of EA do not exist in winter precipitation.

165 This spatial distribution indicates that summer precipitation mainly affects dry/wet conditions in north of EA and the east of CA belonging to the regions of simultaneous rain and heat periods, which is in contrast to the core region of CA. In relation to winter precipitation, the center of the positive value is located in the core region of CA and north of EA, showing the significant contribution of winter precipitation to CA (Fig. 2d). It is worth noting that a certain degree of similarities exists in both summer and winter precipitation of EA and CA, indicating the impact of seasonal precipitation on the linkage of dry/wet conditions in EA

170 and CA at short-term timescales.
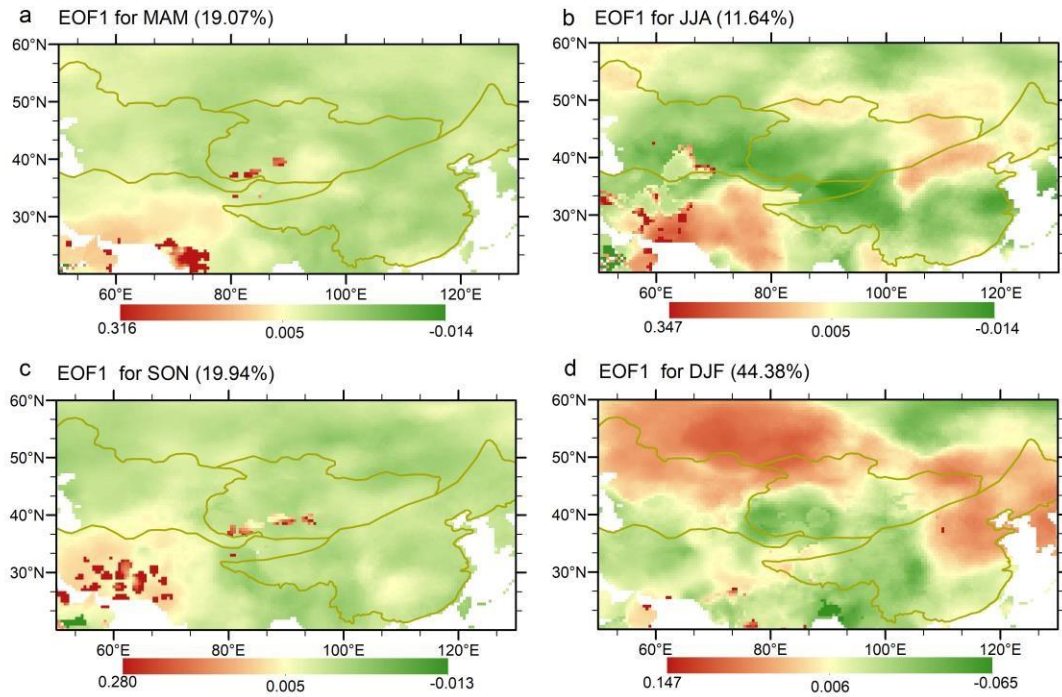
Figure 2. The first EOF modes of precipitation in spring (March, April, and May, MAM) (a), summer (June, July, and August, JJA) (b), autumn (September, October, and November, SON) (c), and winter (December, January, and February, DJF) (d) in EA and CA over 1971-2020.

175 Existing studies emphasized the role of water vapor sources in affecting interannual to interdecadal variability of precipitation (Chen and Huang, 2012; Huang et al., 2015a; Peng and Zhou, 2017; Wei et al., 2017). Therefore, by analyzing the EOF results of water vapor content in the whole layer, this study investigates the general characteristics of the spatial distribution of water vapor in EA and CA and discusses the mechanisms controlling seasonal signals on dry/wet conditions in EA and CA at short-term timescales. The EOF1 of the mean annual water vapor shows that the core region of CA is dominated by positive values, while both

180 EA and the east of CA have negative values (Fig. 3a). The same spatial distribution mode is also reflected in the EOF1 of water vapor difference between summer and winter half-year. To summarize, the water vapor in EA and CA shows a dipole out-of-phase pattern between the simultaneous region of rain and heat periods and the non-simultaneous region of rain and heat periods (Fig. 3b). This implies that the content and source of water vapor are the important reason why dry/wet states in the east of CA is linked to that in EA by seasonal signals of precipitation.
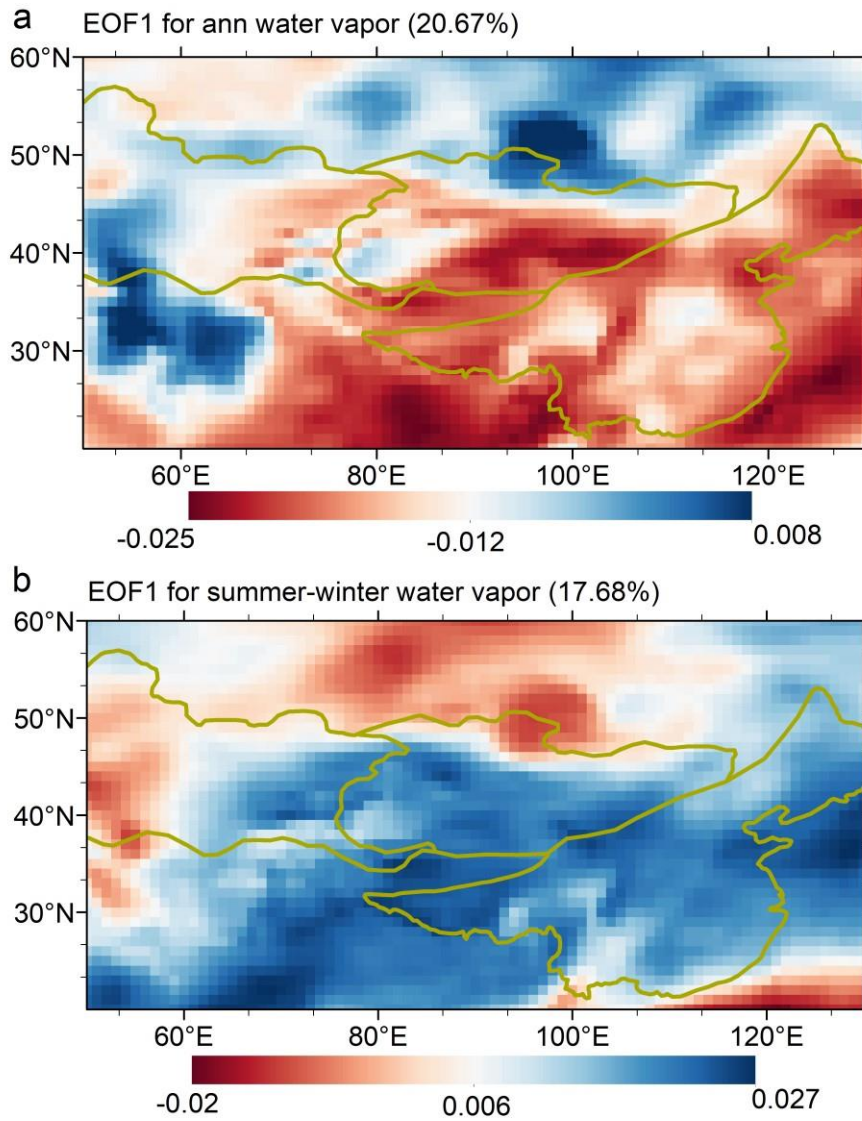
Figure 3. a, the EOF1 modes of annual mean integral water vapor in EA and CA over 1979-2018; b, the EOF1 modes of integral water vapor difference between summer and winter in EA and CA over 1979-2018.

3.2 Spatiotemporal variation of dry/wet conditions and seasonal signals on long timescales

In the last decade, many paleoclimate records with a relatively high resolution, reliable chronology, and robust proxies

190 have been published to discuss the long-term timescale climate evolution in EA and CA. Forty-two moisture records from

individual sites are used to illustrate the spatiotemporal pattern of dry/wet conditions during the LGM, EH, MH, and LH in

EA and CA (Fig. 4). During the LGM, most regions in EA and CA are in moderately dry condition (Fig. 4a). However,

moderately wet and wet conditions partly exist in the east of CA. According to the model simulation, Yu et al. (2000)

concluded that the low temperature in the cold period causes decreasing evaporation, with the enhanced westerlies driven by

expanding land ice sheets, forming the high

195 lake levels in western China and the low lake levels in eastern China during the LGM. During the early Holocene (EH), CA was

dominated by a dry climate, while EA was moderately wet (Fig. 4b). At the same time, there were many records in the east of

CA showing similar dry/wet changes than in EA. During the MH, wet conditions mainly occur in the core region of CA

gradually turning into moderately wet and even dry conditions in the east of CA, while the EA remains moderately wet (Fig.

4c). By the late Holocene (LH), the EA is characterized by dry conditions, while CA is wet (Fig. 4d). In particular, the dry

condition during the

200 LGM and the wet climate during the EH and MH also reflect another meaning of seasonal signals derived from the simultaneity

of rain and heat periods at long-term timescales, namely the "dry-cold" pattern and "wet-warm" pattern.
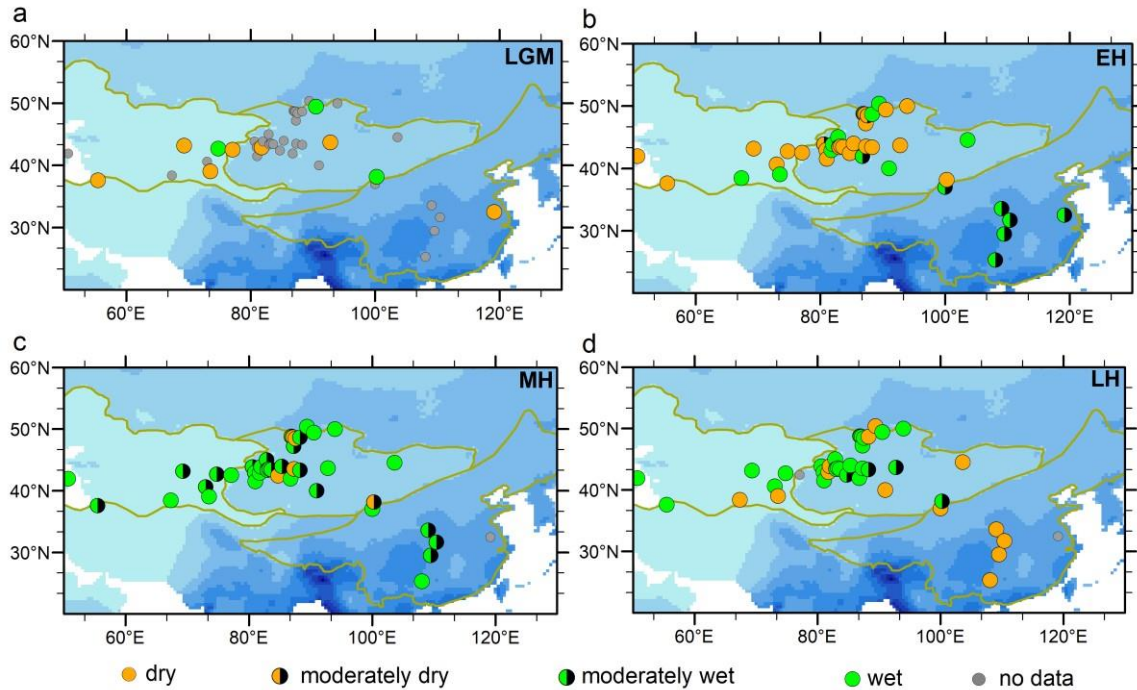
Figure 4. Spatio-temporal characteristics of dry/wet conditions from 42 records since the LGM, based on the confirmation of original
investigators during the LGM, early Holocene (EH), mid Holocene (MH), and late Holocene (LH). Records with an incomplete stage are
shown by a gray dot. Four summarized levels of dry/wet conditions: wet, moderately wet, moderately dry, and dry.

In detail, we further performed a comparative analysis of the time series of typical proxy records in EA and CA (Fig. 5). The

reconstructed precipitation records covering the past 22,600 years from Achit Nuur suggests wet conditions prevailing from

22,600 to 13,200 cal BP (Fig. 5c). Pollen data from the Caspian Sea, controlled by the westerlies, entail that the terrestrial

vegetation around the Caspian Sea changed from desert/desert steppe to dry shrubland/forest over the last ~12,000 years

during the Holocene,

210 revealing the continuous wetting process since the EH and the wettest LH (Fig. 5a). Meanwhile, results of climatically-sensitive

magnetic properties from the Xinjiang loess demonstrate that the relatively wet conditions are generally formed after ~6,000

cal BP, with the wettest climate occurring during the LH (Fig. 5b) (Chen et al., 2016). However, there are inconsistencies

related to dry/wet changes at long-term timescales in the east of CA, which are different from core regions of CA but similar

to EA. Herzschuh.

(2006) analyzed 75 paleoclimatic records in CA and revealed that wet conditions occurred during the EH

215 and MH, while the LGM was characterized by the dry climate (Fig. 5h), indicating the similarity with the monsoon climate

represented by the speleothem $\delta^{18}O$ records from Dongge Cave and Hulu Cave (Fig. 5d). High precipitation in the EH and

MH, indicated by $\delta^{18}O$ records of ostracod shells from Qinghai Lake, shows that the climate in Qinghai Lake since the late

glacial reflects the monsoon-dominated characteristic (Fig. 5e). The climate in Ulaan Nuur is wettest during the EH, humid

during the MH and dry in the LH, embodying a typical characteristic of the East Asian summer monsoon (Fig. 5f). Based on

220 the sediment cores from Lake Karakul and Lake Issyk-Kul, the EH and MH are characterized by wetter conditions in the region,

and the lake level remained low during the LGM (Fig. 5g and j). Furthermore, the regional climate in western China, inferred

from the speleothem oxygen-carbon isotope data from the Kesang Cave, suggests a close coupling with the Asian summer

monsoon (Fig. 5i). The lake level and climate reconstructed results also showed that the "dry-cold" pattern triggered a

substantial lowering of lake level in most of arid western China, challenging the view of "wet-cold" pattern and high lake

levels during

225 the LGM (Zhao et al., 2015).
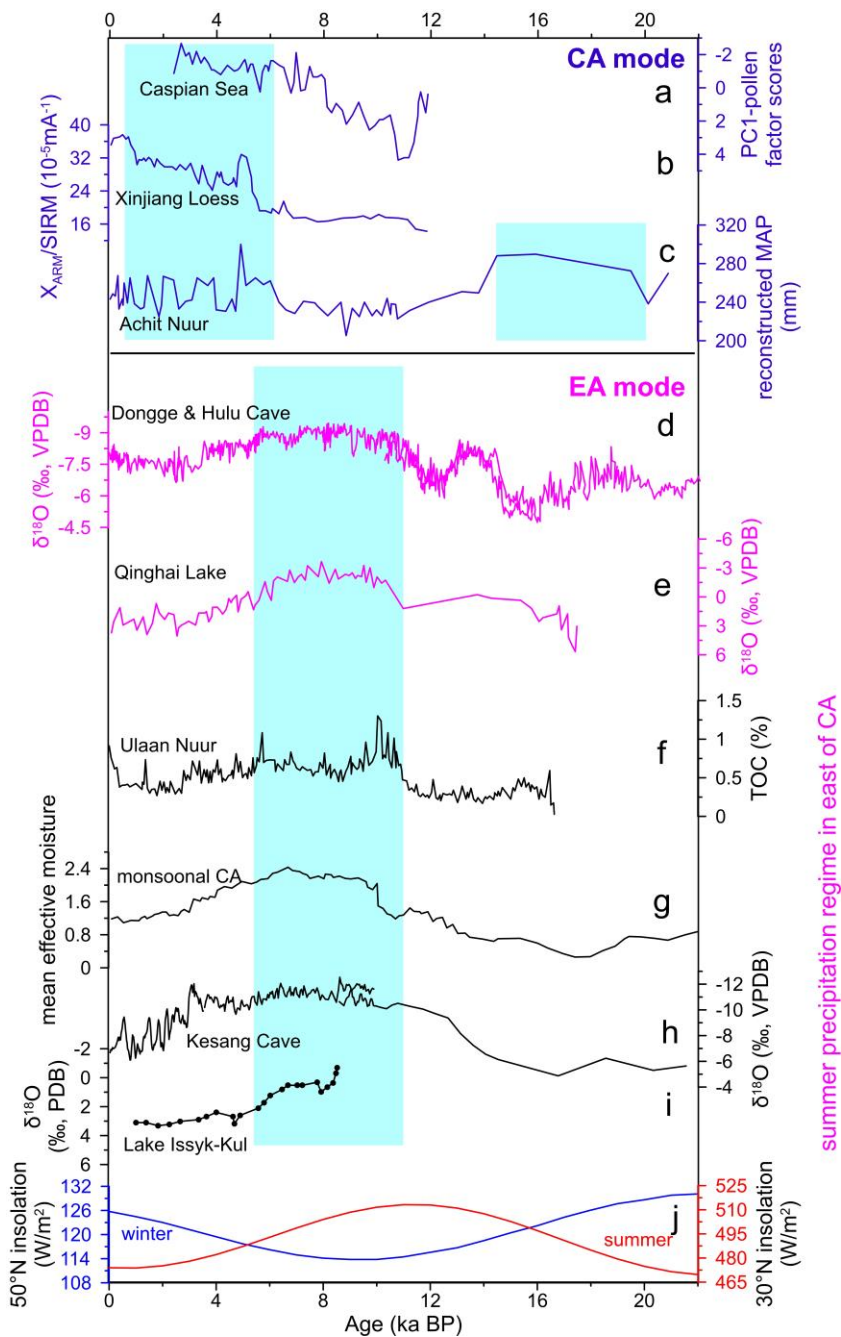
Figure 5. A comparison of proxy variability recorded in EA and CA. a Pollen record from the Caspian Sea (Leroy et al., 2014); b
X_{ARM}/SIRM in the LJW10 section of the Xinjiang Loess (Chen et al., 2016); c Reconstructed MAP (mean annual precipitation) from Achit
Nuur (Sun et al., 2013); d speleothem $\delta^{18}O$ values records from Dongge Cave and Hulu Cave (Yuan et al., 2004; Wang et al., 2001); e $\delta^{18}O$
of ostracode shells from Qinghai Lake (Liu et al., 2007); f TOC (Total organic carbon) from Ulaan Nuur (Lee et al., 2013); g Mean
effective moisture from monsoonal Central Asia (Herzschuh, 2006); h $\delta^{18}O$ from Kesang Cave (Cheng et al., 2016); i $\delta^{18}O$ from Lake
Issyk-Kul (Ricketts et al., 2001); j Summer (red line) insolation at 30°N and winter (blue line) insolation at 50°N (Berger, 1978). Blue
shadows indicate the wet period of paleoclimate proxies.

4 Discussion

4.1 Possible dynamics of seasonal signals on short timescales

EOF analysis of precipitation and water vapor consistently indicates that a connection between EA and the east of CA exists

under the traditional differentiation between EA and the core region of CA. Considering that the east of CA is controlled by the summer precipitation regime. Therefore, we propose that seasonal signals of precipitation contribute to the connection between EA and the east of CA.

240
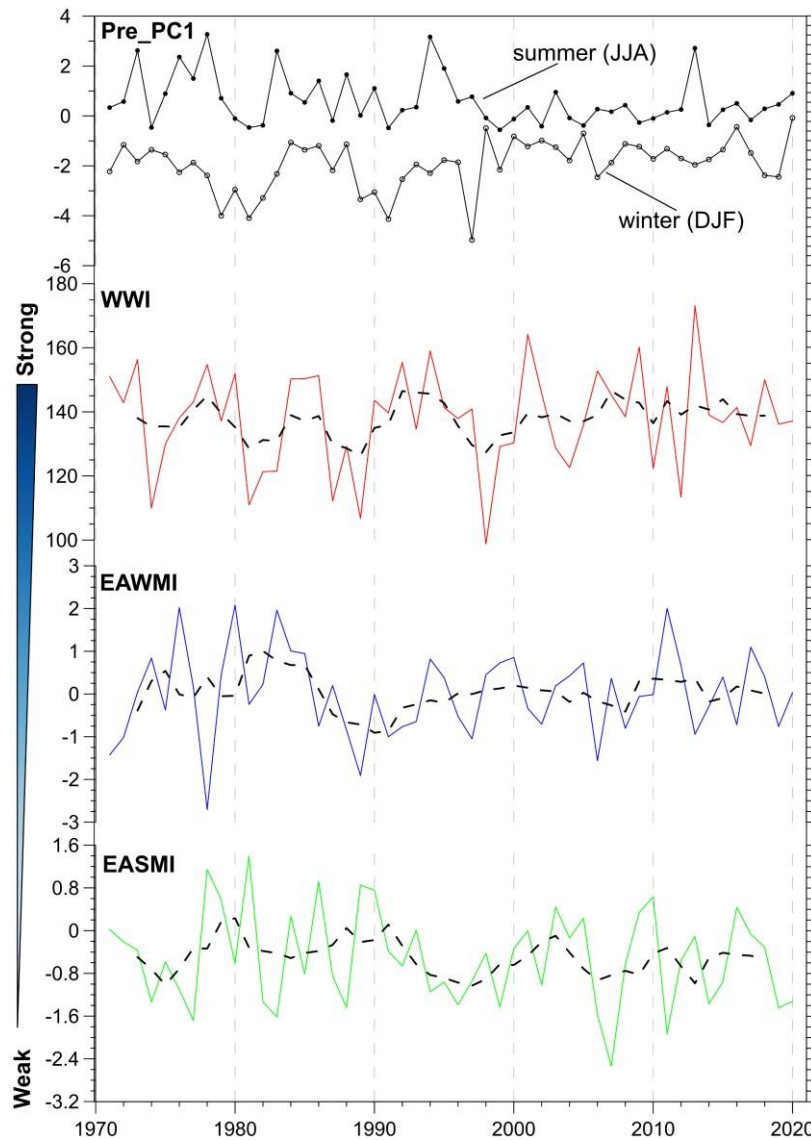
Figure 6. The time series of the precipitation PC1 in summer, winter, WWI, EAWMI, and EASMI over 1971-2020.

Generally, atmospheric circulation has important effects on the spatial distribution and the transportation of water vapor. In order to explore the influence of the modern air-sea circulation on the summer and winter precipitation, we analyzed the time series of the precipitation PC1, WWI, EAWMI, EASMI, NAO, PDO, and ENSO over 1971 to 2020 (Fig. 6 and 7).

245 Comparing the winter precipitation PC1 with WWI and EAWMI (Fig. 6), the weakening of the westerlies and winter monsoons is usually accompanied by an increase in winter precipitation. However, there is not a significant relationship between PC1 of summer precipitation and EASMI. As shown in Figure. 7, summer PDO and ENSO are basically similar to winter PDO and ENSO. However, the markable discrepancy exists in the evolution of winter NAO and summer NAO. The NAO and ENSO indices represent interannual variation, whereas the PDO index has an interdecadal cycle. The NAO index and the winter precipitation PC1 have a positive correlation, suggesting that the North Atlantic may have certain effects on the winter

precipitation through the air-sea interaction. Positive values of the NAO index are usually accompanied by stronger midlatitude westerlies and increased water vapor content from the North Atlantic. The ENSO change, however, were related to the summer precipitation PC1. Winter and summer precipitation before 1980s showed a gradual increasing trend, while PDO values showed a gradual decreasing trend. On the contrary, PDO showed a positive phase when winter and summer precipitation enhanced at interdecadal timescales during 1980-2000. Since the 2000s, the development of winter and summer precipitation was not connected with PDO.
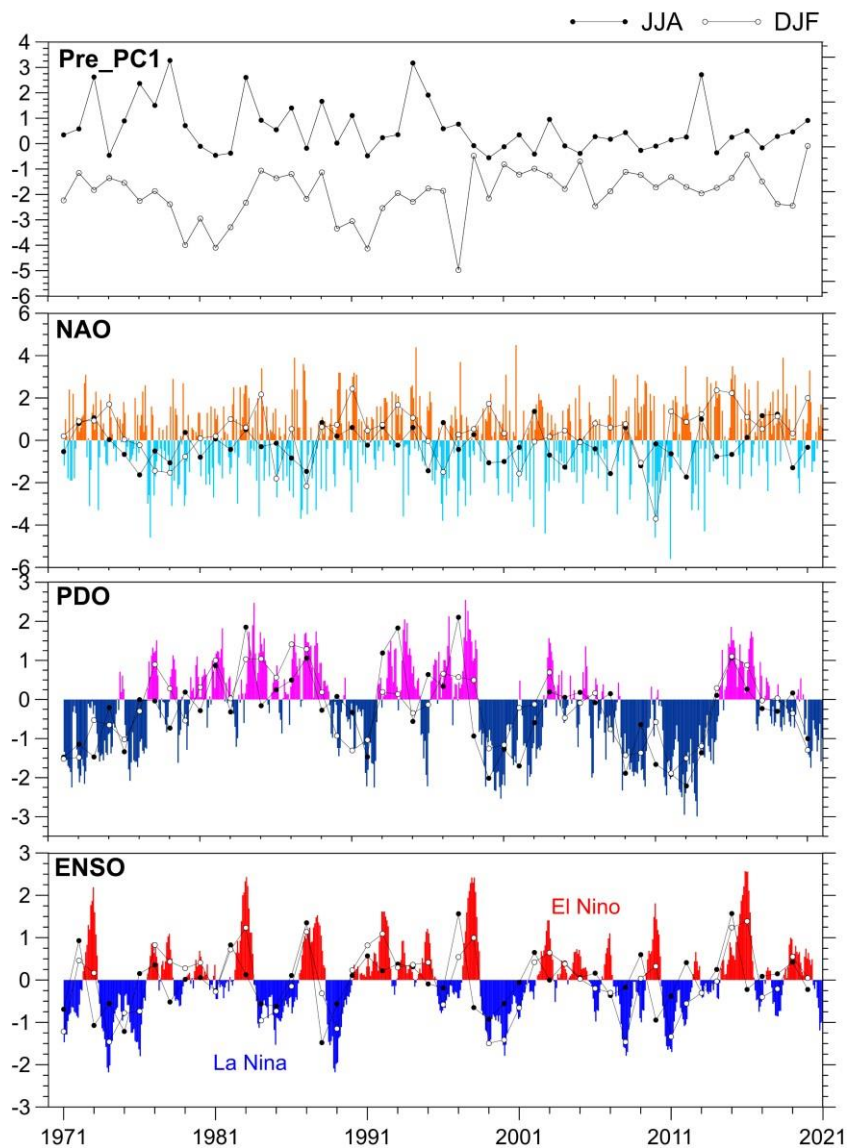
Figure 7. The time series of the precipitation PC1 in summer, winter, and annual mean, NAO, PDO, and ENSO over 1971-2020.

A majority of relevant studies suggest that precipitation variations in CA are controlled by water vapor transported by the midlatitude westerlies, where the monsoonal water vapor source is hard to reach (Huang et al., 2015a; Guan et al., 2019). Abundant moisture is carried from the polar airmass, North Atlantic and the eastern Mediterranean Sea to CA and continues to diffuse

260 eastward to reach the arid region of northwest China (Lioubimtseva, 2014). Meanwhile, several studies in recent years found that

the anti-phase pattern between the East Asian summer monsoon and the westerlies causes the seesaw phenomenon of precipitation variation in northwest China (the east of CA in this study) (Zhang et al., 2019; Wu et al., 2019). However, Chen et al. (2021a) proposed that the East Asian summer monsoon plays an important role in the interdecadal variability of summer precipitation in CA through the transportation of summer water vapor from the Indian and Pacific Oceans to the east of CA. Additionally, Huang et al. (2015b) stated that increased summer precipitation in the Tarim Basin, which belongs to the east of CA, is mainly related to a weakened Indian summer monsoon. In addition, the large-scale topography, such as the Qinghai Tibet Plateau, causes the westerlies to flow around the plateau rather than over it, which in turn influences the local transport of water vapor and results in local precipitation changes (Xie et al., 2014). Therefore, the atmospheric circulation and topographic factors bear on the transportation and content of water vapor at short-term timescales, which differentiates summer precipitation in the east of CA

270 from that in the core region of CA, by linking it to EA.

4.2 Possible dynamics of seasonal signals at long-term timescales

Model simulations are a valid means to visually study mechanisms of paleoclimate change in EA and CA during the LGM and the MH. The results of paleoclimate simulations in this work may help to explain the differences and similarities in dry/wet conditions from EA and CA under the framework of seasonal signals at long-term timescales. During the LGM, lower summer insolation increases the

275 meridional temperature difference and sea level pressure in the summer largely (Fig. 5j; 8a and c), leading to the strengthening of the westerlies (Fig. 9a) and further increasing precipitation in CA (Fig. 8e). However, summer precipitation in EA was weaker than in the MH during the LGM (Fig. 8e) due to the weakening of summer monsoon (Fig. 9c) under the influence of reduced summer insolation (Fig. 5j), which is consistent with dry/wet conditions reconstructed by paleoclimate records in EA (Fig. 5). Besides, although the westerlies weaken during LGM winters (Fig. 9b), the higher winter insolation contributes to the general warming in mid-latitudes

280 (Fig. 5k; 8b), resulting in lower relative humidity in CA (Fig. 8d). According to climatological theory (Barry and Richard, 2009), a decrease in relative humidity entails an increase in saturated water vapor pressure, which ultimately leads to increasing precipitation. Therefore, winter precipitation during the LGM in CA is generally higher than during the MH (Fig. 8f). This relationship may help explaining the asynchrony of long-term dry/wet changes in EA and CA controlled by variations at a seasonal scale.
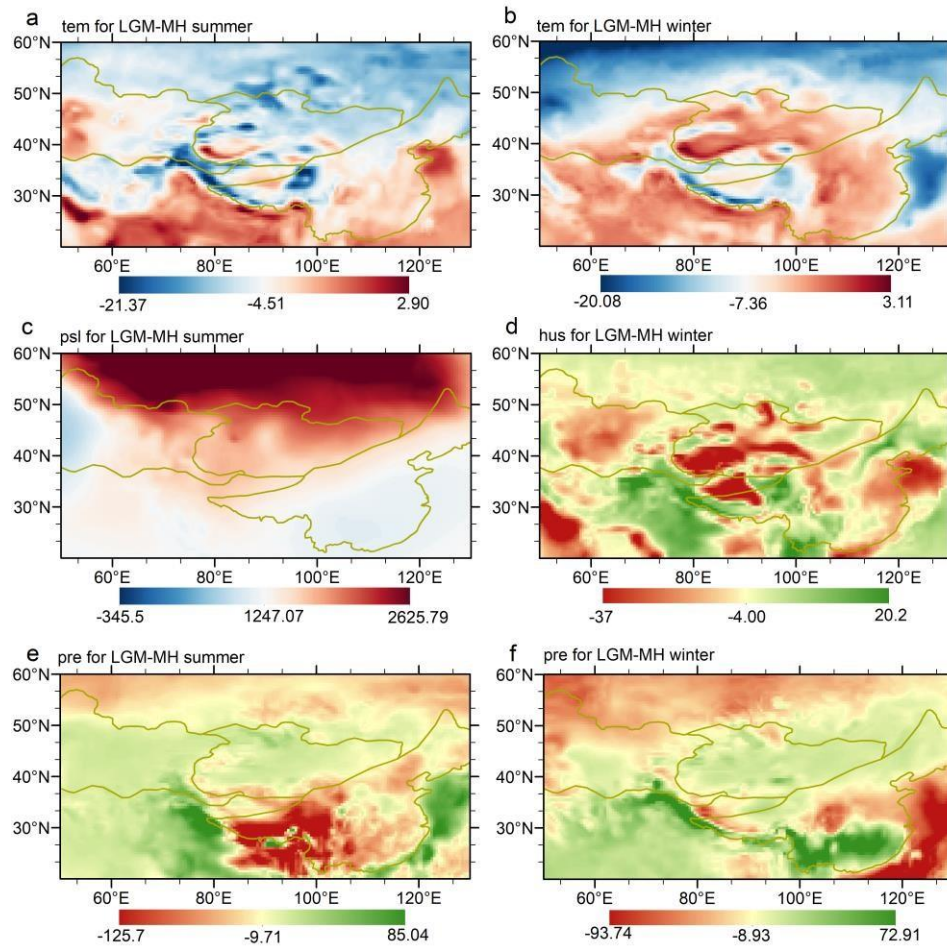
Figure 8. Summer differences of temperature (tem) (a), sea level pressure (psl) (c), and precipitation (pre) (e) for LGM-MH; and winter differences of temperature (b), relatively humid (hus) (d), and precipitation (f) for LGM-MH in EA and CA based on the PMIP3-CMIP5 multi-model ensemble.

Investigating the past climate is key to informing future climate change (Tierney et al., 2020). From the perspective of paleoclimatology, monsoon and westerlies vary greatly between LGM and MH, modulated by primary forces such as orbital insolation, greenhouse gas, and ice sheets (Oster et al., 2015; Bereiter et al., 2015; Sime et al., 2016). Paleoclimate records indicate wet conditions during the LGM and LH in CA and the MH wet in EA (Fig. 5). Specifically, dry/wet conditions in CA, affected by the westerlies and characterized by wet climate states during the LGM and mid- and late-Holocene, is opposite to that in monsoon-dominated EA. However, the proxy records in CA similar to the monsoon evolution are located in the modern summer precipitation region (Figure. 5f-i). From the perspective of precipitation seasonality, there are two different precipitation regimes within CA. The core region of CA has a Mediterranean climate (winter precipitation regime), with a dry summer and seasonal precipitation from early winter to late spring (Fig. 1); whereas, in the east of CA, including northwest of China and west and south of Mongolia, the summer precipitation contributes more (summer precipitation regime; Fig. 1). Therefore, the summer precipitation regime may be a potential forcing factor for the linkage of paleoclimate reconstructions between EA and the east of CA, and the difference in precipitation regime may result in a divergent moisture history in EA and the core region
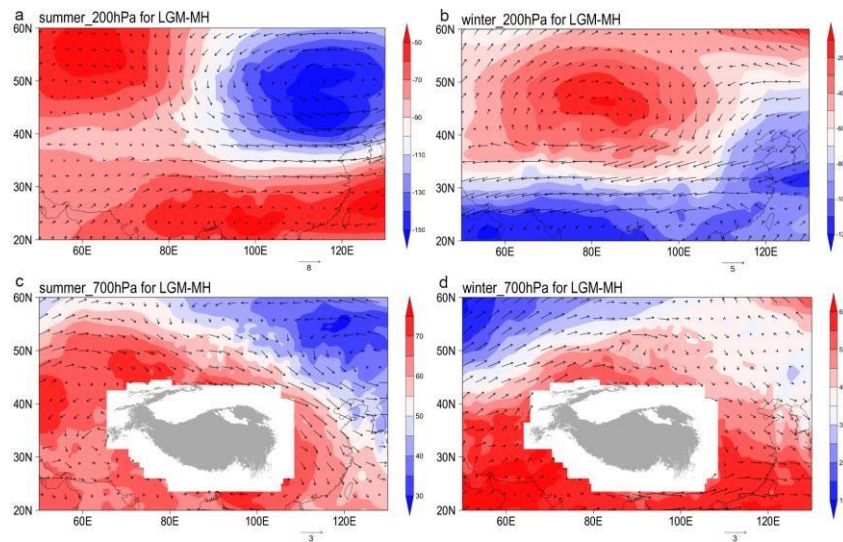
Figure 9. Summer differences of 200 hPa wind field (a) and 700 hPa wind field (c) for LGM-MH; and winter differences of 200 hPa wind field (b) and 700 hPa wind field (d) for LGM-MH in EA and CA based on the PMIP3-CMIP5 multi-model ensemble.

In summary, our results support the notion that seasonal signals of precipitation derived from simultaneous rain and

305 heat periods govern the difference and linkage of dry/wet changes in EA and CA on seasonal to orbital time scales. With global warming and continued increase in winter solar radiation, we suggest that the core region of CA could face a persistent reduction in precipitation in the future. Meanwhile, the decrease in summer solar radiation could lead to a strengthening and southward shift of the summer westerly jet stream over CA, potentially increasing summer precipitation in the east of CA, which is characterised by summer precipitation regimes. However, more quantitative analyses are required to understand how future interannual variations in

310 atmospheric and oceanic circulation might control the seasonal precipitation signals that influence dry/wet changes in the east of CA. Some recent work also points out increasing summer precipitation in arid CA (Chen et al., 2021a; Ren et al., 2022). Meanwhile, the phenomenon of warmer and wetter climates coincides with the simultaneity of rain and heat periods (Hu and Han, 2022). Future work should focus on the fusion of multiple datasets and high-precision climate simulation designed to evaluate the mechanisms of climate change in the region.

315 **5 Conclusion**

The summer precipitation regime in EA and the east of CA and the winter precipitation regime in the core region of CA reveal seasonal signals of precipitation. Using the EOF method, this study analyzes the spatiotemporal variations of precipitation in EA and CA. Results reveal that seasonal signals derived from the simultaneity of rain and heat periods are important factors linking climate change modes in EA and CA at short timescales. A compilation of 42 proxy records with reliable

320 chronologies enable us to reassess the long-term dry/wet changes in EA and CA since the LGM. In core regions of CA, the dry/wet status is

usually characterized by dry EH and wet LH. However, part of records in the east of CA with simultaneous rain and heat

periods show the same dry/wet conditions as in EA, i.e., the dry condition during the LGM and the wet climate during the

EH and MH. This also reflects another meaning of seasonal signals at long-term timescales, namely the "dry-cold" pattern

and "wet-warm" pattern. Concurrently, paleoclimate records reflect seasonal signals triggered by the insolation at long

timescales.

325 The multi-model ensemble simulations of multiple climatic elements may help to explain the climate mechanism of differences and linkage

in dry/wet status from EA and CA since the LGM. Results show that summer insolation influences the meridional

temperature gradient and sea level pressure in the summer, changing the intensity of the westerly winds and summer

monsoon and further controlling the summer precipitation in EA and the east of CA. Meanwhile, winter insolation

contributes to the general warming in EA and the core region of CA, and in turn results in lower relative humidity, which

ultimately increases winter

330 precipitation during the LGM.

In general, the seasonal signals of precipitation derived from the simultaneity and non-simultaneity of rain and heat periods

on short-term timescales can also affect the dry/wet status on long-term timescales, but their influencing factors are different.

Due to the influence of seasonal precipitation signals at multiple time scales, CA and EA controlled by the winter

precipitation regime and the summer precipitation regime, respectively, show an anti-phase evolution of dry/wet changes.

However, it is worth noting

335 that in the east of CA with simultaneous rain and heat events, there is the same dry/wet evolution as in EA. Therefore, we believe that

seasonal signals can provide important insight for analyzing the differences and linkages in climate change between CA and

EA at multiple time scales.

340

345

350

355

235 **Code/Data availability.** The TraCE-21ka dataset comes from the Climate Data Gateway National Center for Atmos pheric

236 Research (NCAR) website at https://www.earthsystemgrid.org/project/trace. html. PMIP3/CMIP5 simulations ar e available

237 from the Earth System Grid Federation (ESGF) Peer-to-Peer (P2P) enterprise system website at https://e sgf-

238 node.llnl.gov/projects/esgf-llnl/. The PDO data can be obtained at https://www.ncei.noaa.gov/pub/data/cmb/ersst/v5

239 /index/ersst.v5.pdo.dat. The Niño 3.4 data can be obtained at https://psl.noaa.gov/gcos_wgsp/Timeseries/Nino34/. The NAO

240 data can be obtained at https://climatedataguide.ucar.edu/sites/default/files/2022-10/nao_station_monthly.txt.

241 **Author contributions.** YL initiated the work. YL and SP conceived the manuscript. SP finished the data sorting, statistical

242 and geospatial data analysis, visualizations of the work, the original draft preparation, and editing and revising of this

243 manuscript. ZZ, MG, XC, JD, YX revised the manuscript.

244 **Competing interests.** The authors declare no competing financial interests.

245 **Acknowledgments.** We acknowledge Simon Jung and two anonymous referees for constructive comments.

246 **Financial support.** This work was supported by the Second Tibetan Plateau Scientific Expedition and Research Program

247 (STEP) (Grant No.2019QZKK0202), the National Natural Science Foundation of China (Grant Nos. 42371159, 42077415).

References

249 An, C., Feng, Z., Barton, L.: 2006. Dry or humid? Mid-Holocene humidity changes in arid and semi-arid China, Quat. Sci.

250   Rev., 25, 351-61, https://doi.org/10.1016/j.quascirev.2005.03.013, 2006.

251 An, C., Lu, Y., Zhao, J., Tao, S., Dong, W., Li, H., Jin, M., Wang, Z.: A high-resolution record of Holocene environmental

252   and climatic changes from Lake Balikun (Xinjiang, China): implications for central Asia, Holocene, 22, 43-52,

253   https://doi.org/10.1177/0959683611405244, 2012.

254 Barichivich, J., Osborn, T. J., Harris, I., van der Schrier, G., Jones, P. D. Monitoring global drought using the self-calibrating

255   Palmer Drought Severity Index [in "State of the Climate in 2020"], B. Am. Meteorol. Soc., 101, S51-S52, 2021.

256 Barry, R. G. and Richard, J. C.: Atmosphere, weather and climate, Routledge, https://doi.org/10.4324/9780203871027, 2009.

257 Bereiter, B., Eggleston, S., Schmitt, J., Nehrbass-Ahles, C., Stocker, T. F., Fischer, H., Kipfstuhl, S., Chappellaz, J.: Revision

258   of the EPICA Dome C CO_2 record from 800 to 600 kyr before present, Geophys. Res. Lett., 42, 542-549,

259   https://doi.org/10.1002/2014GL061957, 2015.

260 Blyakharchuk, T. A., Wright, H. E., Borodavko, P. S., van der Knaap, W. O., Ammann, B.: Late glacial and Holocene

vegetational history of the Altai mountains (southwestern tuva republic, siberia), Palaeogeogr. Palaeoclimatol. Palaeoecol., 245, 518-534, https://doi.org/10.1016/j.palaeo.2006.09.010, 2007.

Briegleb, B. P., Bitz, C. M., Hunke, E. C., Lioscomb, W. H., Holland, M. M., Schramm, J. L., Moritz, A. R.: Scientific

385   description of the sea ice component in the community climate system model, Version 3, 70, https://doi.org/10.5065/D6HH6H1P, 2004.

Cai, Y., Tan, L., Cheng, H., An, Z., Edwards, R. L., Kelly, M. M., Kong, X., Wang, X.: The variation of summer monsoon precipitation in central China since the last deglaciation, Earth Planet. Sci. Lett., 291, 21-31, https://doi.org/10.1016/j.epsl.2009.12.039, 2010.

390   Chen, C., Zhang, X., Lu, H., Jin, L., Du, Y., Chen, F.: Increasing summer precipitation in arid central Asia linked to the weakening of the East Asian summer monsoon in the recent decades, Int. J. Climatol., 41, 1024-1038, https://doi.org/10.1002/joc.6727, 2021a.

Chen, F., Yu, Z., Yang, M., Ito, E., Wang, S., David, B. M., Huang, X., Zhao, Y., Sato, T., Birks, H. J. B., Boomer, I., Chen, J., An, C., Wünnemann, B.: Holocene moisture evolution in arid Central Asia and its out-of-phase relationship with Asian

395   monsoon history, Quat. Sci. Rev., 27, 351-364, https://doi.org/10.1016/j.quascirev.2007.10.017, 2008.

Chen, F., Chen, J., Huang, W.: A discussion on the westerly-dominated climate model in mid-latitude Asia during the modern interglacial period, Earth Sci. Front., 16, 23-32, 2009. (in Chinese with English abstract)

Chen, F., Xu, Q., Chen, J., Birks, H. J. B., Liu, J., Zhang, S., Jin, L., An, C., Telford, R. J., Cao, X., Wang, Z., Zahng, X., Selvaraj, K., Lü, H., Li, Y., Zheng, Z., Wang, H., Zhou, A., Dong, G., Zhang, J., Huang, X., Bloemendal, J., Rao, Z.: East

400   Asian summer monsoon precipitation variability since the last deglaciation, Sci. Rep., 5, 11186, https://doi.org/10.1038/srep11186, 2015.

Chen, F., Jia, J., Chen, J., Li, G., Zhang, X., Xie, H., Xia, D., Huang, W., An, C.: A persistent Holocene wetting trend in arid central Asia, with wettest conditions in the late Holocene, revealed by multi-proxy analyses of loess-paleosol sequences in Xinjiang, China, Quat. Sci. Rev., 146, 134-146, https://doi.org/10.1016/j.quascirev.2016.06.002, 2016.

405   Chen, G. and Huang, R.: Excitation mechanisms of the tele-connection patterns affecting the July precipitation in North-west China, J. Clim., 25, 7834-7851, 2012.

Chen, F., Chen, J., Huang, W., Chen, S., Huang, X., Jin, L., Jia, J., Zhang, X., An, C., Zhang, J., Zhao, Y.: Westerlies Asia and monsoonal Asia: spatiotemporal differences in climate change and possible mechanisms on decadal to suborbital timescales, Earth Sci. Rev., 192, 337-354, https://doi.org/10.1016/j.earscirev.2019.03.005, 2019.

410   Chen, F., Chen, J., Huang, W.: Weakened East Asian summer monsoon triggers increased precipitation in Northwest China,

Sci. China Earth Sci., 64, 835-837, https://doi.org/10.1007/s11430-020-9731-7, 2021b.

Chen, S., Liu, J., Wang, X., Zhao, S., Chen, J., Qiang, M., Liu, B., Xu, Q., Xia, D., Chen, F.: Holocene dust storm variations over northern China: transition from a natural forcing to an anthropogenic forcing, Sci. Bull., 66, 2516-2527, https://doi.org/10.1016/j.scib.2021.08.008, 2021c.

415 Chen, S., Chen, J., Lv, F., Liu, X., Huang, W., Wang, T., Liu, J., Hou, J., Chen, F.: Holocene moisture variations in arid central Asia: Reassessment and reconciliation, Quat. Sci. Rev., 297, 107821, https://doi.org/10.1016/j.quascirev.2022.107821, 2022.

Cheng, H., Zhang, P., Spötl, C., Edwards, R. L., Cai, Y., Zhang, D., Sang, W., Tan, M., An, Z.: The climatic cyclicity in semiarid-arid central Asia over the past 500,000 years, Geophys. Res. Lett., 39, L01705,

420   https://doi.org/10.1029/2011gl050202, 2012.

Cheng, H., Spötl, C., Breitenbach, S. F. M., Sinha, A., Wassenburg, J. A., Jochum, K. P., Scholz, D., Li, X., Peng, Y., Lv, Y., Zhang, P., Votintseva, A., Loginov, V., Ning, Y. F., Kathayat, G., Edwards, R. L.: Climate variations of Central Asia on orbital to millennial timescales, Sci. Rep., 6, 36975, Climate variations of Central Asia on orbital to millennial timescales, 2016.

425 Dykoski, C. A., Edwards, R. L., Cheng, H., Yuan, D., Cai, Y., Zhang, M., Lin, Y., Qing, J., An, Z., Revenaugh, J.: A high-resolution, absolute-dated Holocene and deglacial Asian monsoon record from Dongge Cave, China, Earth Planet. Sci. Lett., 233, 71-86, https://doi.org/10.1016/j.epsl.2005.01.036, 2005.

Feng, Z., Sun, A., Abdusalih, N., Ran, M., Kurban, A., Lan, B., Zhang, D., Yang, Y.: Vegetation changes and associated climatic

changes in the southern Altai Mountains within China during the Holocene, Holocene, 27, 683-693,

430   https://doi.org/10.1177/0959683616670469, 2016.

Gao, F., Jia, J., Xia, D., Lu, C., Lu, H., Wang, Y., Liu, H., Ma, Y., Li, K.: Asynchronous Holocene climate optimum across midlatitude Asia, Palaeogeogr. Palaeoclimatol. Palaeoecol., 518, 206e214, https://doi.org/10.1016/j.palaeo.2019.01.012, 2019.

Gent, P. R., Danabasoglu, G., Donner, L. J., Holland, M. M., Hunke, E. C., Jayne, S. R., Lawrence, D. M., Neale, R. B., Rasch,

435   P. J., Vertenstein, M.: The community climate system model version 4, J. Clim., 24, 4973-4991, https://doi.org/10.1175/2011jcli4083.1, 2011.

Guan, X., Yang, L., Zhang, Y., Li, J.: Spatial distribution, temporal variation, and transport characteristics of atmospheric water

vapor   over   Central Asia   and   the   arid   region   of   China,   Global   Planet.   Change,   172,   159-178,

https://doi.org/10.1016/j.gloplacha.2018.06.007, 2019.

440 Han, S., Wu, N., Li, Z.: Inland climate changes in Dzungaria during the late Pleistocene Epoch, Geog. Res., 12, 47-54, 1993.

(in Chinese with English abstract).

Han, S. and Qu, Z.: Inland Holocene climatic features recorded in Balikun lake, northern Xinjiang. Science in China Series B-

Chemistry, Life Sciences & Earth Sciences, 11, 1201-1209, 1992. (in Chinese with English abstract)

Harris, I., Jones, P. D., Osborn, T. J., Lister, D. H.: Updated high-resolution grids of monthly climatic observations-the CRU

445 TS3.10 Dataset, Int. J. Climatol., 34, 623-642, 2014.

Heinecke, L., Mischke, S., Adler, K., Barth, A., Biskaborn, B. K., Plessen, B., Ingmar, N., Gerhard, K., Ilhomjon, R.,

Herzschuh, U.: Climatic and limnological changes at Lake Karakul (Tajikistan) during the last ~29 cal ka, J.

Paleolimnol., 58, 317334, https://doi.org/10.1007/s10933-017-9980-0, 2017.

Hersbach, H., Bell, B., Berrisford, P., Hirahara, S., Horányi, A., Muñoz-Sabater, J., Nicolas, J., Peubey, C., Radu, R., Schepers,

450 D., Simmons, A., Soci, C., Abdalla, S., Abellan, X., Balsamo, G., Bechtold, P., Biavati, G., Bidlot, J., Bonavita, M., De Chiara, G.,

Dahlgren, P., Dee, D., Diamantakis, M., Dragani, R., Flemming, J., Forbes, R., Fuentes, M., Geer, A., Haimberger, L.,

Healy, S., Hogan, J. R., Holm, E., Janiskova, M., Keeley, S., Laloyaux, P., Lopez, P., Lupu, C., Radnoti,

G., de Rosnay, P., Rozum, I., Vamborg, F., Villaume, S., Thepaut, J.: The ERA5 global reanalysis, Q. J. Roy. Meteor.

Soc., 146, 1999-2049, https://doi.org/10.1002/qj.3803, 2020.

455 Herzschuh, U.: Palaeo-moisture evolution in monsoonal central Asia during the last 50,000 years, Quat. Sci. Rev., 25, 163-178, https://doi.org/10.1016/j.quascirev.2005.02.006, 2006.

Hu, Q. and Han, Z.: Northward Expansion of Desert Climate in Central Asia in Recent Decades, Geophys. Res. Lett., 49, e2022GL098895, https://doi.org/10.1029/2022gl098895, 2022.

Huang, W., Chen, J., Zhang, X., Feng, S., Chen, F.: Definition of the core zone of the "westerlies-dominated climatic regime",

460 and its controlling factors during the instrumental period, Sci. China Earth Sci., 58, 676-684, https://doi.org/10.1007/s11430-015-5057-y, 2015a.

Huang, W., Feng, S., Chen, J., Chen, F.: Physical mechanisms of summer precipitation variations in the Tarim basin in northwestern China, J. Clim., 28, 3579-3591, https://doi.org/10.1175/jcli-d-14-00395.1, 2015b.

Huang, X., Chen, F., Fan, Y., Yang, M.: Dry late-glacial and early Holocene climate in arid central Asia indicated by lithological 465 and palynological evidence from Bosten Lake, China. Quat. Int., 194, 19-27, https://doi.org/10.1016/j.quaint.2007.10.002,

2009.

Hurrell, J. W. and Deser, C.: North Atlantic climate variability: The role of the North Atlantic Oscillation, J. Mar. Syst., 78, 28-

41, https://doi.org/10.1016/j.jmarsys.2008.11.026, 2009.

Hurrell, J. W.: Decadal Trends in the North Atlantic Oscillation: Regional Temperatures and Precipitation, Science, 269, 676-

470   679, https://doi.org/10.1126/science.269.5224.676, 1995.

Jia, J., Chen, J., Wang, Z., Chen, S., Wang, Q., Wang, L., Yang, L., Xia, D., Chen, F.: No evidence for an anti-phased

Holocene moisture regime in mountains and basins in Central Asian: records from Ili loess, Xinjiang, Palaeogeogr.

Palaeoclimatol. Palaeoecol., 572, 110407, https://doi.org/10.1016/j.palaeo.2021.110407, 2021.

Jiang, Q., Ji, J., Shen, J., Matsumoto, R., Tong, G., Qian, P., Ren, X., Yan, D.: Holocene vegetational and climatic variation in

475   westerly-dominated areas of Central Asia infrred from the Sayram Lake in northern Xinjiang, China, Sci. China Earth

Sci., 56, 339-353, https://doi.org/10.1007/s11430-012-4550-9, 2013.

Jiang, Q., Meng, B., Wang, Z., Qian, P., Zheng, J., Jiang, J., Zhao, C., Hou, J., Dong, G., Shen, J., Liu, W., Liu, Z., Chen, F.:

Exceptional terrestrial warmth around 4200-2800 years ago in Northwest China, Sci. Bull., 67, 427-436,

https://doi.org/10.1016/j.scib.2021.11.001, 2022.

480   Joussaume, S., Taylor, K. E., Braconnot, P. J. F. B., Mitchell, J. F. B., Kutzbach, J. E., Harrison, S. P., Prentice, I. C.,

Broccoli, A. J., Abe-Ouchi, A., Bartlein, P. J., Bonfils, C.: Monsoon changes for 6000 years ago: results of 18 simulations from the

paleoclimate   modeling   intercomparison   project   (PMIP),   Geophys.   Res.   Lett.,   26,   859-862,

https://doi.org/10.1029/1999gl900126, 1999.

Kang, S., Wang, X., Roberts, H. M., Duller, G. A., Song, Y., Liu, W., Zhang, R., Liu, X., Lan, J.: Increasing effective moisture

485   during the Holocene in the semiarid regions of the Yili Basin, central Asia: evidence from loess sections, Quat. Sci. Rev.,

246, 106553, https://doi.org/10.1016/j.quascirev.2020.106553, 2020.

Lee, M. K., Lee, Y. I., Lim, H. S., Lee, J. I., Yoon, H. I.: Late Pleistocene-H olocene records from Lake Ulaan, southern

Mongolia: implications for east Asian palaeomonsoonal climate changes, J. Quat. Sci., 28, 370-378,

https://doi.org/10.1002/jqs.2626, 2013.

490   Leroy, S. A., López-Merino, L., Tudryn, A., Chalié, F., Gasse, F.: Late Pleistocene and Holocene palaeoenvironments in and

around the middle Caspian basin as reconstructed from a deep-sea core, Quat. Sci. Rev., 101, 91-110,

https://doi.org/10.1016/j.quascirev.2014.07.011, 2014.

Leroy, S. A. G., Ricketts, R. D., Rasmussen, K. A.: Climatic and limnological changes 12,750 to 3600 years ago in the Issyk-

Kul catchment, Tien Shan, based on palynology and stable isotopes, Quat. Sci. Rev., 259, 106897,

495   https://doi.org/10.1016/j.quascirev.2021.106897, 2021.

Leroy, S. A. G., Lopez-Merino, L., Tudryn, A., Chalie, F., Gasse, F.: Late Pleistocene and Holocene palaeoenvironments in and around the middle Caspian basin as reconstructed from a deep-sea core, Quat. Sci. Rev., 101, 91-110, https://doi.org/10.1016/j.quascirev.2014.07.011 2014.

Li, J.: The patterns of environmental changes since last Pleistoc ene in northwestern China, Quat. Sci., 3, 197-204, 1990. (in Chinese with English abstract)

Li, X., Zhao, K., Dodson, J., Zhou, X.: Moisture dynamics in central Asia for the last 15 kyr: new evidence from Yili Valley, Xinjiang, NW China, Quat. Sci. Rev., 30, 3457-3466, https://doi.org/10.1016/j.quascirev.2011.09.010, 2011.

Li, Y., Song, Y., Kaskaoutis, D. G., Zan, J., Orozbaev, R., Tan, L., Chen, X.: Aeolian dust dynamics in the Fergana Valley, Central Asia, since~30 ka inferred from loess deposits, Geosci. Front., 12, 101180, https://doi.org/10.1016/j.gsf.2021.101180, 2021.

Li, Y., Song, Y., Orozbaev, R., Dong, J., Li, X., Zhou, J.: Moisture evolution incentral Asia since 26 ka: insights from a Kyrgyz loess section, western tian Shan, Quat. Sci. Rev. 249, 106604, https://doi.org/10.1016/j.quascirev.2020.106604, 2020a.

Li, Y., Peng, S., Liu, H., Zhang, X., Ye, W., Han, Q., Zhang, Y., Xu, L., Li, Y.: Westerly jet stream controlled climate change mode since the Last Glacial Maximum in the northern Qinghai-Tibet Plateau, Earth Planet. Sci. Lett., 549, 116529, https://doi.org/10.1016/j.epsl.2020.116529, 2020b.

Lioubimtseva, E.: Impact of Climate Change on the Aral Sea and its Basin. The Devastation and Partial Rehabilitation of a Great Lake, The Aral Sea, 405-427, https://doi.org/10.1007/978-3-642-02356-9_17, 2014.

Liu, X., Shen, J., Wang, S., Wang, Y., Liu, W.: Southwest monsoon changes indicated by oxygen isotope of ostracode shells from sediments in Qinghai lake since the late glacial, Chin. Sci. Bull., 4, 109-114, https://doi.org/10.1007/s11434-007-0086-3, 2007.

Liu, X., Liu, J., Shen, C., Yang, Y., Chen, J., Chen, S., Wang, X., Wu, C., Chen, F.: Inconsistency between records of $\delta^{18}O$ and trace element ratios from stalagmites: evidence for increasing midelate Holocene moisture in arid central Asia, Holocene, 30, 369-379, https://doi.org/10.1177/0959683619887, 2020.

Lorenz, E.: Empirical orthogonal function and statistical weather prediction. Scientific Report No. 1 Statist Forecasting Project.

Department of Meteorology, Massachusetts Institute of Technology, 1956.

Manoj, M. C., Srivastava, J., Uddandam, P. R., Thakur, B.: A 2000 year multiproxy evidence of natural/anthropogenic influence on climate from the southwest coast of India, J. Earth Sci., 31, 1029-1044, https://doi.org/10.1007/s12583-020-1336-4, 2020.

Mantua, N. J. and Hare, S. R.: The Pacific Decadal Oscillation, J. Oceanogr., 58, 35-44, https://doi.org/10.1023/A:1015820616384, 2002.

Mischke, S., Lai, Z., Aichner, B., Heinecke, L., Makhmudov, Z., Kuessner, M. L., Herzschuh, U.: Radiocarbon and optically stimulated luminescence dating of sediments from Lake Karakul, Tajikistan, Quat. Geochronol., 41, 51-61, https://doi.org/10.1016/j.quageo.2017.05.008, 2017.

Nagashima, K., Tada, R., Tani, A., Sun, Y., Isozaki, Y., Toyoda, S., Hasegawa, H.: Millennial-scale oscillations of the westerly jet path during the last glacial period, J. Asian Earth Sci., 40, 1214-1220, https://doi.org/10.1016/j.jseaes.2010.08.010, 2011.

Peltier, W. R.: Global glacial isostasy and the surface of the ice-age Earth: The ICE-5G (VM2) model and GRACE, Annu. Rev.

Earth Planet. Sci., 32, 111-149, https://doi.org/10.1146/annurev.earth.32.082503.144359, 2004.

Peng, D. and Zhou, T.: Why was the arid and semiarid North-west China getting wetter in the recent decades, J. Geophys. Res. Atmos., 122, 9060-9075, https://doi.org/10.1002/2016JD026424, 2017.

Ran, M. and Feng, Z.: Variation in carbon isotopic composition over the past ca. 46,000 yr in the loessepaleosol sequence in central Kazakhstan and paleoclimatic significance, Org. Geochem., 73, 47-55, https://doi.org/10.1016/j.orggeochem.2014.05.006, 2014.

Randall, D. A., Wood, R. A., Bony, S., Colman, R., Taylor, K. E.: Climate models and their evaluation. In Climate change 540 2007: The physical science basis. Contribution of Working Group I to the Fourth Assessment Report of the IPCC (FAR) (pp. 589-662), Cambridge University Press, 2007.

Rayner, N. A. A., Parker, D. E., Horton, E. B., Folland, C. K., Alexander, L. V., Rowell, D. P., Kent, E. C.: Global analyses of sea surface temperature, sea ice, and night marine air temperature since the late nineteenth century, J. Geophys. Res. Atmos., 108, 4407, https://doi.org/10.1029/2002jd002670, 2003.

Ren, Y., Yu, H., Liu, C., He, Y., Huang, J., Zhang, L., Hu, H., Zhang, Q., Chen, S., Liu, X., Zhang, M., Wei, Y., Yang, Y., Fan, W., Zhou, J.: Attribution of Dry and Wet Climatic Changes over Central Asia, J. Clim., 35,1399-1421, https://doi.org/10.1175/jcli-d-21-0329.1, 2021.

Ricketts, R. D., Johnson, T. C., Brown, E. T., Rasmussen, K. A., Romanovsky, V. V.: The Holocene paleolimnology of Lake Issyk-Kul, Kyrgyzstan: trace element and stable isotope composition of ostracodes, Palaeogeogr. Palaeoclimatol. 550 Palaeoecol., 176, 207-227, https://doi.org/10.1016/s0031-0182(01)00339-x, 2001.

Rotstayn, L., Collier, M., Dix, M., Feng, Y., Gordon, H., O'Farrell, S., Smith, I., Syktus, J.: Improved simulation of Australian climate and ENSO-related climate variability in a GCM with an interactive aerosol treatment, Int. J. Climatol., 30, 10671088, https://doi.org/10.1002/joc.1952, 2010.

Rudaya, N., Tarasov, P., Dorofeyuk, N., Solovieva, N., Kalugin, I., Andreev, A., Daryin, A., Diekmann, B., Riedel, F., 555 Tserendash, N., Wagner, M.: Holocene environments and climate in the Mongolian Altai reconstructed from the Hoton-Nur pollen and diatom records: a step towards better understanding climate dynamics in Central Asia, Quat. Sci. Rev., 28, 540-554, https://doi.org/10.1016/j.quascirev.2008.10.013, 2009.

Schmidt, G. A., M. Kelley, L. Nazarenko, R. Ruedy, G. L. Russell, I. Aleinov, M. Bauer, S. E. Bauer, M. K. Bhat, R. Bleck, V. Canuto, Y. Chen, Y. Cheng, T. L. Clune, A. Del Genio, R. de Fainchtein, G. Faluvegi, J. E. Hansen, R. J. Healy, N. Y. 560 Kiang, D. Koch, A. Lacis, A. N. LeGrande, J. Lerner, K. K. Lo, E. E. Matthews, S. Menon, R. L. Miller, V. Oinas, A. O. Oloso, J. P. Perlwitz, M. J. Puma, W. M. Putman, D. Rind, A. Romanou, M. Sato, D. Shindell, S. Sun, R. A. Syed, N. Tausnev, K. Tsigaridis, N. Unger, A. Voulgarakis, M. Yao, J. Zhang.: Configuration and assessment of the GISS ModelE2 contributions to the CMIP5 archive, J. Adv. Modeling Earth Syst., 6, 141-184, https://doi.org/10.1002/2013MS000265, 2014.

565   Sorg, A., Bolch, T., Stoffel, M., Solomina, O., Beniston, M.: Climate change impacts on glaciers and runoff in Tien Shan (Central Asia), Nature Clim Change, 2, 725-731, https://doi.org/10.1038/nclimate1592, 2012.

Sun, A., Feng, Z., Ran, M., Zhang, C.: Pollen-recorded bioclimatic variations of the last ∼22,600 years retrieved from Achit Nuur core in the western Mongolian Plateau, Quat. Int., 311, 36-43, https://doi.org/10.1016/j.quaint.2013.07.002, 2013.

Tao, S., An, C., Chen, F., Tang, L., Wang, Z., Lü, Y., Li, Z., Zheng, T., Zhao, J.: Pollen-inferred vegetation and environmental 570 changes since 16.7 ka BP at Balikun Lake, Xinjiang, Chin. Sci. Bull., 55, 2449-2457, https://doi.org/10.1007/s11434-010-3174-8, 2010.

Tian, F., Herzschuh, U., Telford, R. J., Mischke, S., Van der Meeren, T., Krengel, M.: A modern pollen-climate calibration set from central-western Mongolia and its application to a late glacial-Holocene record, J. Biogeogr., 41, 1909-1922, https://doi.org/10.1111/jbi.12338, 2014.

575 Tierney, J. E., Poulsen, C. J., Montañez, I. P., Bhattacharya, T., Feng, R., Ford, H. L., Hönisch, B., Inglis, G. N., Petersen, S. V., Sagoo, N., Tabor, C. R., Thirumalai, K., Zhu, J., Burls, N. J., Foster, G. L., Goddéris, Y., Huber, B. T., Ivany, L. C., Kirtland, Turner, S., Lunt, D. J., McElwain, J. C., Mills, B. J. W., Otto-Bliesner, B. L., Ridgwell, A., Zhang, Y.: Past climates inform our future, Science, 370, eaay3701, https://doi.org/10.1126/science.aay3701, 2020.

Voldoire, A., Sanchez-Gomez, E., Mélia, D. S. Y, Decharme, B., Cassou, C., Sénési, S., Valcke, S., Beau, I., Alias, A., 580 Chevallier, M., Déqué, M., Deshayes, J., Douville, H., Fernandez, E., Madec, G., Maisonnave, E., Moine, M. P., Planton, S., Saint-Martin, D., Szopa, S., Tyteca, S., Alkama, R., Belamari, S., Braun, A., Coquart, L., Chauvin, F.: The CNRM-CM5.1 global climate model: description and basic evaluation, Clim. Dyn., 40, 2091-2121, https://doi.org/10.1007/s00382-011-1259-y, 2013.

Wang, B., Liu, J., Kim, H. J., Webster, P. J., Yim, S. Y.: Recent change of the global monsoon precipitation (1979-2008), Clim.

585 Dyn., 39, 1123-1135, https://doi.org/10.1007/s00382-011-1266-z, 2012.

Wang, L., Jia, J., Xia, D, Liu, H., Gao, F., Duan, Y., Wang, Q., Xie, H., Chen, F.: Climate change in arid central Asia since MIS

2 revealed from a loess sequence in Yili Basin, Xinjiang, China, Quat. Int., 502, 258-266, https://doi.org/10.1016/j.quaint.2018.02.032, 2018.

Wang, P., Wang, B., Cheng, H., Fasullo, J., Guo, Z., Kiefer, T., Liu, Z.: The global monsoon across time scales: Mechanisms

590 and outstanding issues, Earth Sci. Rev., 174, 84-121, https://doi.org/10.1016/j.earscirev.2017.07.006, 2017.

Wang, Y., Cheng, H., Edwards, R. L., An, Z., Wu, J., Shen, C., Dorale, J. A.: A high-resolution absolute-dated late Pleistocene

monsoon record from Hulu cave, China, Science, 294, 2345-2348, https://doi.org/10.1126/science.1064618, 2001.

Wang, Q., Wei, H., Khormali, F., Wang, L., Xie, H., Wang, X., Huang, W., Chen, J., Chen, F.: Holocene moisture variations in

western arid central Asia inferred from loess records from NE Iran, G-cubed, 21, e2019GC008616,

595 https://doi.org/10.1029/2019gc008616, 2020.

Watanabe, S., Hajima, T., Sudo, K., Nagashima, T., Takemura, T., Okajima, H., Nozawa, T., Kawase, H., Abe, M., Yokohata,

T., Ise, T., Sato, H., Kato, E., Takata, K., Emori, S., Kawamiya, M.: MIROC-ESM 2010: model description and basic

results of CMIP5-20c3m experiments, Geosci. Model Dev., 4, 845-872, https://doi.org/10.5194/gmd-4-845-2011, 2011.

Wei, W., Zhang, R., Wen, M., Yang, S.: Relationshipbetween the Asian westerly jet stream and summer rainfall over Central

600 Asia and North China: roles of the Indian mon-soon and the south Asian high, J. Clim., 30, 537-552, https://doi.org/10.1175/JCLI-D-15-0814.1, 2017.

Wu, P., Ding, Y., Liu, Y., Li, X.: The characteristics of moisture recycling and its impact on regional precipitation against the

background of climate warming over Northwest China, Int. J. Climatol., 39, 5241-5255, https://doi.org/10.1002/joc.6136, 2019.

605 Xie, C., Li, M., Zhang, X.: Characteristics of summer atmospheric water resources and its causes over the Tibetan plateau in recent 30 years, J. Nat. Resour., 29, 979-989, 2014. (in Chinese with English abstract)

Xu, H., Lan, J., Zhang, G., Zhou, X.: Arid Central Asia saw mid-Holocene drought, Geology, 47, 255-258, https://doi.org/10.1130/g45686.1, 2019.

Yang, Y., Feng, Z., Zhang, D., Lan, B., Ran, M., Wang, W., Sun, A.: Holocene hydroclimate variations in the eastern Tianshan

610 Mountains of northwestern China inferred from a palynological study, Palaeogeogr. Palaeoclimatol. Palaeoecol., 564,

110184, https://doi.org/10.1016/j.palaeo.2020.110184, 2021.

Yu, G., Xue, B., Wang, S., Liu, J.: Chinese lakes records and the climate significance during Last Glacial Maximum, Chin. Sci.

Bull., 45, 250-255, https://doi.org/10.3321/j.issn:0023-074X.2000.03.003, 2000. (in Chinese with English abstract)

Yukimoto, S., Adachi, Y., Hosaka, M., Sakami, T., Yoshimura, H., Hirabara, M., Tanaka, T. Y., Shindo, E., Tsujino, H., Deushi,
615   M. A new global climate model of the Meteorological Research Institute: MRI-CGCM3: Model description and basic

   performance, J. Meteorol. Soc. Japan, 90, 23-64, https://doi.org/10.2151/jmsj.2012-a02, 2012.

Zhang, H., Yu, K., Zhao, J., Feng, Y., Lin, Y., Zhou, W., Liu, G.: East Asian Summer Monsoon variations in the past 12.5 ka:

   High-resolution δ^{18}O record from a precisely dated aragonite stalagmite in central China, J. Asian Earth Sci., 73, 162-

   175, https://doi.org/10.1016/j.jseaes.2013.04.015, 2013.

620   Zhang, J., Nottebaum, V., Tsukamoto, S., Lehmkuhl, F., Frechen, M.: Late Pleistocene and Holocene loess sedimentation in

   central and western Qilian Shan (China) revealed by OSL dating, Quat. Int., 372, 120-129,

   https://doi.org/10.1016/j.quaint.2014.12.054, 2015.

Zhang, J. and Lin, Z.: Climate of China, Wiley, New York, 1992.

Zhang, D., Chen, X., Li, Y., Ran, M., Yang, Y., Zhang, S., Feng, Z.: Holocene moisture variations in the arid central Asia: new
625   evidence from the southern Altai mountains of China, Sci. Total Environ., 735, 139545,

   https://doi.org/10.1016/j.quaint.2014.12.054, 2020.

Zhang, D. and Feng, Z.: Holocene climate variations in the Altai Mountains and the surrounding areas: a synthesis of pollen

   records, Earth Sci. Rev., 185, 847-869, https://doi.org/10.1016/j.earscirev.2018.08.007, 2018.

Zhang, Q., Lin, J., Liu, W., Han, L.: Precipitation seesaw phenomenon and its formation mechanism in the eastern and
western 630 parts of Northwest China during the flood season, Sci. China Earth Sci., 62, 2083-2098, https://doi.org/10.1007/s11430-

   018-9357-y, 2019.

Zhao, Y., An, C., Mao, L., Zhao, J., Tang, L., Zhou, A., Li, H., Dong, W., Duan, F., Chen, F.: Vegetation and climate history in

   arid western China during MIS2: New insights from pollen and grain-size data of the Balikun Lake, eastern Tien Shan,

   Quat. Sci. Rev., 126, 112-125, https://doi.org/10.1016/j.quascirev.2015.08.027, 2015.